GaN/AlN QUANTUM DOT INTRABAND PHOTODETECTORS AT 1.3-1.5 MICRONS

L. Doyennette[1], A. Lupu[1], L. Nevou[1], M. Tchernycheva[1], R. Colombelli[1], F.H. Julien[1], A. Vardi[2], G. Bahir[2], F. Guillot[3], E. Monroy[3]

[1]*Institut d'Electronique Fondamentale, Université Paris-Sud, UMR 8622 CNRS, 91405 Orsay, France*
[2]*Department of Electrical Engineering, Technion-Israel Institute of Technology, Haifa 32000, Israel*
[3] *Equipe Mixte CEA-CNRS-UJF Nanophysique et Semiconducteurs, DRFMC/SP2M/PSC, CEA-Grenoble, 17 rue des Martyrs, 38054 Grenoble cedex 9, France*
(Received 6 October 2006)

Abstract

GaN/AlN quantum dot (QD) photodetectors based on intraband absorption and in-plane carrier transport in the wetting layer have been fabricated and characterized. The devices are operating at room temperature in the wavelength range 1.3-1.5 μm. The dots exhibit TM polarized absorption, linked to the s-p_z transition. The photocurrent at 300K is slightly blue-shifted with respect to the s-p_z intraband absorption. The responsivity increases with temperature and reaches a record value of 8 mA/W at 300 K for detectors with interdigitated contacts.

1. Introduction

Existing semiconductor device technologies in the telecommunication wavelength range are dominated by interband devices such as diode lasers, switches and modulators, and the material system employed is usually InGaAs(P)-on-InP. However, the same wavelength range can be covered with intersubband (ISB) transitions provided that the semiconductor heterostructure exhibits sufficiently high conduction band discontinuity. The extremely short absorption recovery time characteristic of ISB transitions is advantageous for high-speed optoelectronic applications. The operating principles of ISB emitters, detectors, switches and modulators have already been successfully validated at mid- and far-IR wavelengths using semiconductor materials such as GaAs/AlGaAs or InGaAs/AlInAs-on-InP. In order to reduce the operation wavelength to the 1.3-1.55 μm wavelength range, new materials are required.

Group-III nitrides have recently emerged as the most promising candidates for the development of the ISB devices for ultra-high bit–rate optical communications [1]. Apart from the wide band gap, these materials also offer a huge conduction band offset (~1.7 eV for GaN/AlN heterostructures) allowing us to tune the ISB transition to near-infrared domain. Room-temperature ISB absorptions at $\lambda \approx 1.3\text{-}1.55$ μm have been observed by several groups in highly-doped GaN/Al(Ga)N quantum wells (QWs) grown by molecular beam epitaxy [2-4] or metalorganic vapour phase epitaxy [5-7], and in GaN/AlN quantum dots (QDs) [8, 9].

Quantum dots are of great interest for intraband photodetection [10, 11]. As compared to QW intersubband photodetectors, they should exhibit an intrinsically lower noise due to the reduction of electron-phonon scattering. Secondly, normal incidence photodetection is allowed because of the three-dimensional electronic confinement in the QDs. Regular quantum dot infrared photodetectors (QDIPs) are based on vertical transport of electrons. The photoex-

cited electrons tunnel into the continuum towards the contact under an applied bias. For in-plane QDIPs, the confined electrons are excited into the two-dimensional wetting layer (WL) and the photocurrent (PhC) relies on lateral carrier transport. In-plane QDIPs have already been demonstrated in InAs/GaAs QDs [12].

In this paper, we report on GaN/AlN QDIPs based on intraband absorption and lateral carrier transport in the WL, operating at wavelengths as short as 1.37 μm at room temperature [13, 14]. The responsivity is peaked at 1.41 μm wavelength and is as high as 8mA/W at room temperature for the interdigitated contact photodetector.

2. Sample growth

Three QDIPs have been investigated (further labelled S1, S2, and S3). All samples consist of 20 periods of Si-doped GaN QD layers separated by 3 nm-thick AlN barriers. They are grown on 1 μm thick AlN buffer on *c*-sapphire substrate by plasma-assisted molecular-beam epitaxy. Electron population of the QDs is provided by silicon doping of the GaN layer at a nominal concentration of 1×10^{20} cm^{-3}. An additional QD layer is deposited on the sample surface to allow atomic force microscopy (AFM) characterizations of the QD size and density. Further growth details are given elsewhere [16]. A scheme of the sample structure as well as an AFM image of the QDs on the surface are shown in Fig. 1. The QD density is in the range $4.6\text{-}6.8\times10^{11}$ cm^{-2} for all the samples. The measured QD height is about 1.2-1.3 nm and the diameter ranges from 15 to 17 nm.

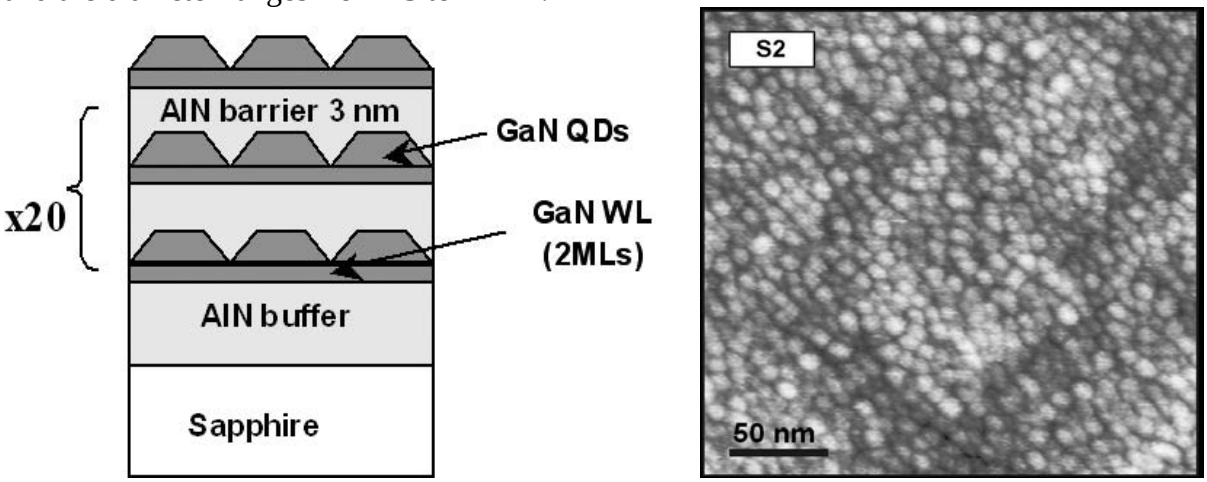

Figure 1: Left: sample structure scheme. Right: AFM image of the QDs synthesized on the surface of the S2 sample.

3. Device fabrication

The sample facets have been mechanically polished at a 45° angle to form a multi-pass waveguide with 5-6 total internal reflections for optical characterizations. Two types of contacts have been fabricated as illustrated in Fig. 2. For samples S1 and S2, the two metal contacts with a size of 900x3000 μm are separated by 800 μm and annealed at 600°C for 30 sec. For sample S3, interdigitated metal contacts were deposited. They consist of ten 800-μm-long and 20-μm-wide fingers, separated by 10 or 20 μm. In all the cases, the metal contacts were defined by standard photolithography and the deposited metal layers are Ti/Al/Ti/Au. The linear current-voltage characteristics of the samples indicate an ohmic behavior.

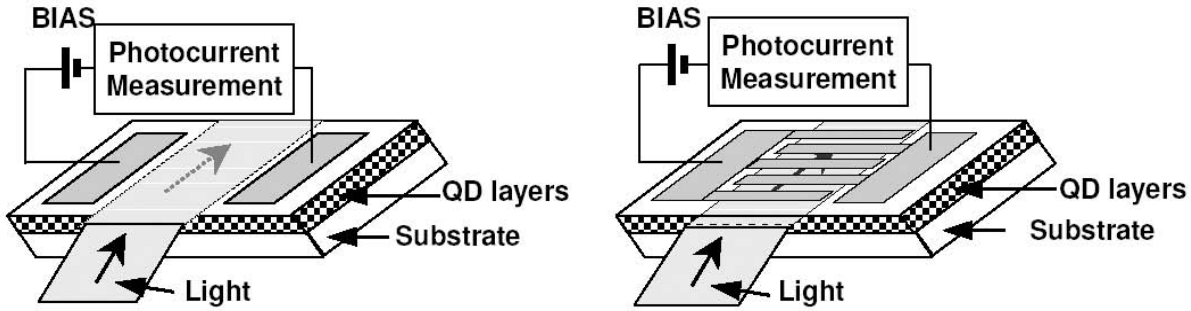

Figure 2: Schematic of the two types of photodetectors. Left: two metal contacts (900x3000 μm) separated by 800 μm (samples S1 and S2). Right: 20 μm wide interdigitated metal contacts separated by 10 μm or 20 μm (sample S3).

4. Experimental results and discussion

Samples have been first characterized by photoluminescence (PhL) and Fourier transform infrared (FTIR) spectroscopies to ascertain the optical transition energies. The PhL measurements were performed at room temperature using the 244 nm line of a frequency-doubled CW Ar^{++} laser. The PhL signal is peaked at 3.78 eV, 3.63 eV and 3.9 eV for S1, S2 and S3 samples, respectively. These values are typical of dots with a height of 1-1.3 nm [14] and thus are consistent with the AFM measurements. The full width at half maximum (FWHM) is less than 300 meV for the three samples indicating a good size homogeneity. Indeed, a variation of 1 monolayer of the QD height leads to a shift of ~150 meV of the peak PhL energy.

The intraband absorption of the samples was deduced from the transmission measurements carried out in a multi-pass waveguide configuration with 5-6 total internal reflections. The intraband absorptions are peaked at 1.42 μm (0.87 eV), 1.67 μm (0.74 eV), and 1.48 μm (0.84 eV) for samples S1, S2, and S3, respectively. Fig. 3 presents the absorption spectra of the samples S1 and S2. The absorption resonances are only observed for TM-polarized light. Based on the polarization selection rules, the observed absorptions are ascribed to the intraband transitions from the ground electronic state (*s*-shell) to the excited state with one node of the envelope function along the c-axis (p_z-shell) [9]. The absorptions from the ground state to the in-plane excited states (p_x or p_y) are not observed in the investigated energy range, probably because their energies are below the cut-off of the sapphire substrate (0.3 eV). The QD parameters deduced from the AFM measurements, PhL and intraband absorption energies are summarized in Table I.

For the room-temperature photocurrent (PhC) measurements, the infrared light of the FTIR spectrometer was injected onto the 45° angle facet and the detected photocurrent was amplified using a current amplifier. For S1 and S2 samples with surface contacts, PhC measurements were performed under a continuous bias of 5 V using a lock-in detection and the step scan operating mode to increase the sensivity. For sample S3 with interdigitated contacts, the applied bias was 10V, and the intraband photocurrent was fed directly into the FTIR operating in rapid scan mode. The PhC energy peaks for each sample are indicated in Table I.

The PhC spectra for S1 and S2 samples are shown in Fig. 3. The PhC signal is only observed for TM-polarized light following the polarization selection rule of the s-p_z intraband absorption. The fact that the PhC follows the intraband absorption spectrum and obeys the same selection rules is a clear evidence that it originates from the intraband transition in the QDs. The confined electrons undertake the intraband transition, then are transferred to the WL

Table I: Density, height and diameter of the quantum dots of samples S1, S2 and S3. The PhL energy, the intraband transition energy and the photocurrent are also indicated for each sample.

	QD Density ($x10^{11}cm^{-2}$)	Height (nm)	Diameter (nm)	PhL energy (eV)	Intraband energy and wavelength [FWMH]	Photocurrent energy and wavelength (eV)
S1	6.4±0.7	1.2±0.6	17	3.821	0.856eV 1.45μm	0.9eV 1.37μm
S2	4.6±0.5	1.3±0.6	16	3.78	0.74eV 1.67μm	0.85eV 1.46μm
S3	6.8±0.5	1.2±0.5	15	3.63	0.84eV 1.47μm	0.88eV 1.41μm

and experience in-plane transport. It should be noted that the photocurrent spectra of Fig. 3 are slightly blueshifted with respect to the *s*-p_z intraband absorption and that the blueshift increases with the peak wavelength of the detectors. One likely explanation supported by energy state calculations [15] is that the p_z shell has a lower energy than the WL ground state.

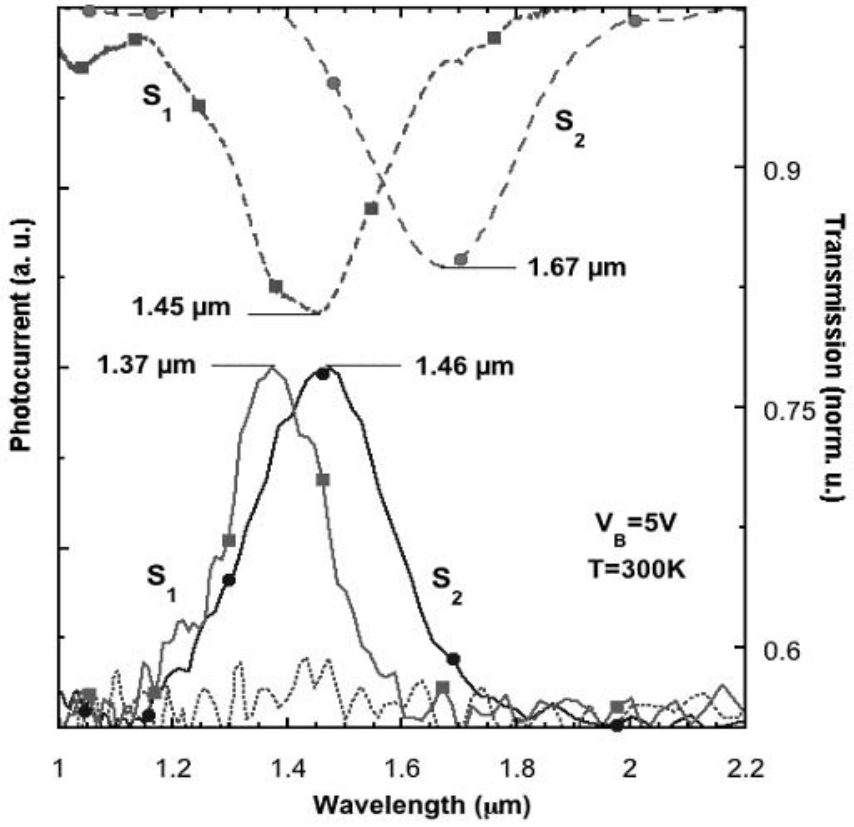

Figure 3: Room temperature transmission (dashed line) and photocurrent spectra (full line) for samples S1 and S2. The dotted curve shows the photocurrent for TE-polarized incident light.

The photoexcited electrons transfer to the WL ground state via phonon absorption. Since the difference of energy between the WL and the p_z state is larger for big dots than for small dots, the phonon assisted mediated mechanism favours the smaller dots in the distribution. This mechanism explains the blueshift of the PhC with respect to the absorption, and

also why the blueshift increases with the peak wavelength of the detection. This interpretation is also supported by the temperature dependence of the PhC.

Figure 4 shows the transmission and the PhC spectra at various temperatures of sample S3 with interdigitated contacts. As seen, the PhC signal peaked at 1.41 μm wavelength exponentially increases with temperature. Such behaviour is expected for a process involving phonon absorption.

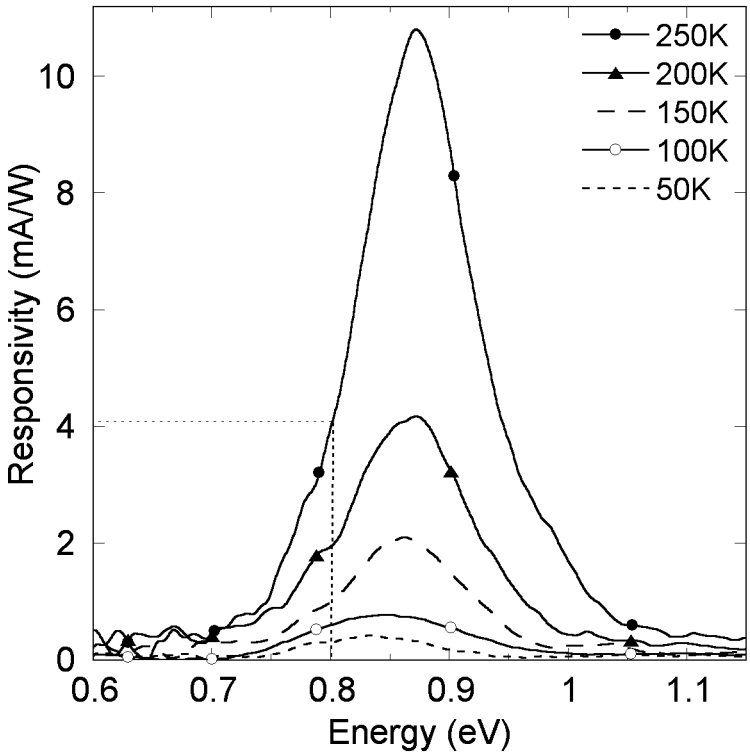

Figure 4: Responsivity of sample S3 with interdigitated contacts. From bottom to top, the temperature of the PhC measurements is respectively 50, 100, 150, 200, 250 K.

The PhC responsivity has been calibrated using a 1.55 μm semiconductor laser. The S3 sample with interdigitated contacts provides the highest responsivity. The responsitivity at 1.41 μm wavelength is about 8 mA/W at 300K.

5. Conclusions

In conclusion, we have demonstrated GaN/AlN quantum dot photodetectors based on intraband absorption and in-plane electronic transport operating at record short wavelength for unipolar devices. The photocurrent is TM-polarized and is generated by the transfer of the photoexcited electrons from the p_z state to the wetting layer. A blueshift of the PhC with respect to the intraband absorption is observed and is interpreted in terms of phonon assisted transfer from the p_z state to the ground state of the wetting layer.

Acknowledgements

The authors would like to acknowledge the financial support of EC FP6 STREP project "Nitwave" under IST contract #004170.

References

[1] M. Tchernycheva, L. Nevou, L. Doyennette, F.H. Julien, E. Warde, F. Guillot, E. Monroy, E. Bellet-Amalric, T. Remmele, M. Albrecht, Phys. Rev. B, 73, 125347, (2006).
[2] C. Gmachl, H.M. Ng, S. N. G. Chu and A.Y. Cho, Appl. Phys. Lett., 77, 3722, (2000).
[3] K. Kishino, A. Kikuchi, H. Kanazava and T. Tachibana, Appl. Phys. Lett., 81, 1234, (2002).
[4] A. Helman, M. Tchernycheva, A. Lusson, E. Warde, F.H. Julien, K. Moumanis, G. Fishman, E. Monroy, B. Daudin, D.L.S. Dang et al., Appl. Phys. Lett., 83, 5196, (2003).
[5] N. Suzuki and N. Iizuka, Jpn. J. Appl. Phys., 38, L363, (1999).
[6] S. Nicolay, J.F. Carlin, E. Feltin, R. Butte, M. Mosca, N. Grandjean, M. Ilegems, M. Tchernycheva, L. Nevou and F.H. Julien, Appl. Phys. Lett., 87, 111106, (2005).
[7] S. Nicolay, E. Feltin, J.-F. Carlin, M. Mosca, L. Nevou, M. Tchernycheva, F.H. Julien, M. Ilegems and N. Grandjean, Appl. Phys. Lett., 88, 151902, (2006).
[8] Kh. Moumanis, A. Helman, F. Fossard, M. Tchernycheva, A. Lusson, F.H. Julien, B. Damilano, N. Grandjean, J. Massies, Appl. Phys. Lett., 82, 868, (2003).
[9] M. Tchernycheva, L. Nevou, L. Doyennette, A. Helman, R. Colombelli, F.H. Julien, F. Guillot, E. Monroy, T. Shibata and M. Tanaka, Appl. Phys. Lett., 87, 101912, (2005).
[10] D. Pal, E. Towe, Appl. Phys. Lett., 88, 153109, (2006).
[11] V. Ryzhii, Semicond. Sci. Technol., 11, 759 (1996).
[12] L. Chu, A. Zrenner, M. Bichler, G. Abstreiter, Appl. Phys. Lett., 79, 2249, (2001).
[13] L. Doyennette, L. Nevou, M. Tchernycheva, A. Lupu, F. Guillot, E. Monroy, R. Colombelli and F.H. Julien, Electron. Lett., 41, 1077, (2005).
[14] A. Vardi, N. Akopian, G. Bahir, L. Doyennette, M. Tchernycheva, L. Nevou, F.H. Julien, F. Guillot, E. Monroy, Appl. Phys. Lett., 88, 143101, (2006).